Numerical modelling of fracture processes in thermal shock weakened rock

Martina Pressacco[1], Timo Saksala[2]

[1]*Laboratory of Civil Engineering, Tampere University of Technology, Tampere, Finland.*
Position: PhD student. Degree: Master of Science. Email address: martina.pressacco@tut.fi
[2]*Position: Academy Research Fellow. Degree: Doctor of Science. Email address: timo.saksala@tut.fi*

Abstract

This paper presents some preliminary results of a research project aiming at the simulation of thermal shock assisted percussive drilling. In the present study, a numerical model for transient thermal shock induced damage in rock is presented. This model includes a rock mesostructure description accounting for different mineral properties and a thermo-mechanical constitutive model based on embedded discontinuity finite elements. In the numerical simulations, the thermal shock induced damge process is first simulated. Then the uniaxial compression test on thermally affected numerical rock samples is carried out. The effect of thermal shock is demonstrated by comparison to uniaxial compression test simulation on intact rock. The results show that the thermal-shock assisted rock breakage is a feasible idea to be extended to percussive drilling as well.

1 Introduction

Weakening the rock by thermal shock is a promising method to facilitate mechanical breakage in traditional drilling or rock crushing. This method consists of damaging the rock first by application of high amplitude heat shock and then applying the mechanical loading. During the last 15 years, some encouraging results have been obtained in numerical modelling of microwave-assisted breakage (Whittles et al., 2003), thermal spallation (Walsh et al., 2013), and plasma torch shocked granite (Mardoukhi et al., 2017).

In this paper, some preliminary results on numerical modelling of heat shocked granite under mechanical loading are presented. For this end, we present a combined thermo-mechanical fracture model to simulate heat-shock induced damage and consequent mechanical breakage. More specifically, the constitutive model for rock is based on the embedded discontinuity finite elements (Saksala et al., 2015), where thermal coupling is taken into account through thermal strains. An explicit time-integration algorithm is presented for solving the global thermo-mechanical problem. The performance of this method is demonstrated in the numerical examples by simulating uniaxial compression tests on thermally affected numerical rock samples.

2 Finite element formulation for the uncoupled thermo-mechanical problem

The aim of this analysis is to model the behavior of a rock sample exposed first to a thermal shock and then subjected to mechanical loading. If the external heat source (which in the present case is a flux **q** applied at the boundaries of the rock specimen) is significantly larger than the heat generation due to the mechanical response, the coupling term in the solution for the heat equation can be neglected. Therefore, for our purposes, the finite element formulation for the heat balance equation becomes

$$\mathbf{C}\dot{\theta} + \mathbf{K}_\theta \theta - \mathbf{f}_\theta = \mathbf{0} \tag{1}$$

where $\mathbf{C}$, $\mathbf{K}_\theta$ and $\mathbf{f}_\theta$ are the capacity matrix, the conductivity matrix and the external force, respectively, defined as follows:

$$\mathbf{C} = \int_V \rho c \mathbf{N}_\theta^T \mathbf{N}_\theta dV, \qquad \mathbf{K}_\theta = \int_V k \mathbf{B}_\theta^T \mathbf{B}_\theta dV, \qquad \mathbf{f}_\theta = -\int_S q_n \mathbf{N}_\theta^T dS \qquad (2)$$

where ρ is the density, c is the specific heat capacity, θ is the temperature, $\mathbf{N}_\theta$ is the temperature interpolation matrix, k is the conductivity, q_n is the normal component of the external heat flux and finally $\mathbf{B}_\theta$ is the gradient of the temperature interpolation matrix.

In general, both the heat capacity matrix and the conductivity matrix depend on temperature. However, in this preliminary analysis the dependance of the material properties on temperature is neglected.

The mechanical problem is governed by the finite element discretized equation of motion

$$\mathbf{M}\ddot{\mathbf{u}} + \mathbf{f}_{int} = \mathbf{f}_{ext}, \qquad \mathbf{f}_{int} = \int_V \mathbf{B}_u^T \boldsymbol{\sigma} dV \qquad (3)$$

where $\mathbf{M}$ is the lumped mass matrix, $\mathbf{f}_{ext}$ is the external force vector, $\mathbf{B}_u$ is the kinematic matrix and $\boldsymbol{\sigma}$ is the stress vector.

3 Rock mesostructure description

The rock mesostructure is represented as a random mineral grain distribution based on centroidal Voronoi tessellation. The tool adopted for this purpose is the `PolyMesher` Matlab code by (Talischi et al., 2012), which generates centroidal Voronoi tessellations, whereas the FE mesh consists of constant strain three-node triangles. The rock sample is composed of three main minerals, (i.e. quartz, feldspar and biotite), each of them having different mechanical and thermal properties. The FE mesh and the random mineral texture are shown in Figure 1 a) and b). It should be reminded that the Voronoi cells (mineral grains) are meshed with the three-node elements.

4 Rock constitutive model

The model used here adopts the main idea developed in (Saksala et al., 2015), namely the representation of cracks by embedded discontinuity finite elements. According to the adaptation here, the material response is linear elastic until the tensile strength is reached. The fracture criterion adopted here is the Rankine criterion. A discontinuity (crack) is introduced when the first principal stress in the element exceeds the tensile strength. The normal vector $\mathbf{n}$ of the discontinuity is parallel to the first principal stress direction.

The model components, i.e. the loading functions, the evolution laws for discontinuity jump and the internal variable, and the Kuhn-Tucker conditions, can be summarized as:

$$\phi_t(\mathbf{t}_{\Gamma_d}, \kappa, \dot{\kappa}) = \mathbf{n} \cdot \mathbf{t}_{\Gamma_d} - (\sigma_t + q(\kappa, \dot{\kappa})), \qquad \phi_s(\mathbf{t}_{\Gamma_d}, \kappa, \dot{\kappa}) = |\mathbf{m} \cdot \mathbf{t}_{\Gamma_d}| - (\sigma_s + \frac{\sigma_s}{\sigma_t} q(\kappa, \dot{\kappa})) \qquad (4)$$

$$\dot{\boldsymbol{\alpha}}_d = \dot{\boldsymbol{\alpha}}_I + \dot{\boldsymbol{\alpha}}_{II} = \dot{\lambda}_t \frac{\partial \phi_t}{\partial \mathbf{t}_{\Gamma_d}} + \dot{\lambda}_s \frac{\partial \phi_s}{\partial \mathbf{t}_{\Gamma_d}} \qquad (5)$$

$$\dot{\mathbf{t}}_{\Gamma_d} = -\mathbf{E} : (\nabla \phi \otimes \dot{\boldsymbol{\alpha}}_d)^{sym}, \qquad \dot{\kappa} = -\dot{\lambda}_t \frac{\partial \phi_t}{\partial q} - \dot{\lambda}_s \frac{\partial \phi_s}{\partial q} \qquad (6)$$

$$q = h\kappa + s\dot{\kappa}, \qquad h = -g\sigma_t \exp(-g\kappa) \qquad (7)$$

$$\dot{\lambda}_i \geq 0, \qquad \phi_i \leq 0, \qquad \dot{\lambda}_i \phi_i = 0, \qquad i = t, s \qquad (8)$$

where $\mathbf{n}$ and $\mathbf{m}$ are respectively the unit normal and tangent vectors for the crack, σ_t and σ_s are the elastic limits for the stress in tension and shear, and κ, $\dot{\kappa}$ are the internal variable and its rate which relate to the softening law for the discontinuity. The softening slope parameter g is defined with the mode I fracture energy G_{Ic} as $g = \sigma_t/G_{Ic}$, and s is the viscosity modulus. The total displacement jump $\boldsymbol{\alpha}_d$ is decomposed in two parts, $\boldsymbol{\alpha}_I$ and $\boldsymbol{\alpha}_{II}$, correspondent to mode I and II increments, while $\dot{\lambda}_t$ and $\dot{\lambda}_s$ represent the crack opening and sliding increments. The stress tensor assumes the following expression

$$\boldsymbol{\sigma} = \mathbf{E} : \left(\boldsymbol{\varepsilon}_{tot} - (\nabla\phi \otimes \boldsymbol{\alpha}_d)^{sym} - \boldsymbol{\varepsilon}_\theta \right) \tag{9}$$

with $\mathbf{E}$ being the elasticity tensor and

$$\nabla\phi = \arg\left(\max_{k=1,2} \frac{|\sum_{i=1}^k \nabla N_i \cdot \mathbf{n}|}{\| \sum_{i=1}^k \nabla N_i \|} \right), \qquad \boldsymbol{\varepsilon}_\theta = \alpha \Delta\theta \mathbf{I} \tag{10}$$

where ϕ is a function that restricts the effect of the displacement jump within the corresponding finite element so the essential boundary conditions remain unaffected. More details can be found in (Saksala et al., 2015). Moreover, $\boldsymbol{\varepsilon}_\theta$ is the thermal strain, with α being the thermal expansion coefficient.

5 Time integration scheme

By applying the forward Euler scheme $\dot{\boldsymbol{\theta}}_n = (\boldsymbol{\theta}_{n+1} - \boldsymbol{\theta}_n)/\Delta t$ to the FE discretized heat equation (1), the following explicit expression is obtained for solving the temperature

$$\mathbf{C}_n \boldsymbol{\theta}_{n+1} = (\mathbf{C}_n - \Delta t \mathbf{K}_{\theta,n}) \boldsymbol{\theta}_n + \Delta t \mathbf{f}_{\theta,n} \tag{11}$$

which is valid also for nonlinear cases where $\mathbf{C}$ and $\mathbf{K}_\theta$ depend on temperature.

The explicit modified Euler time integration scheme is chosen for the integration of the mechanical part. It is based on solving the acceleration from the equation of motion (3) and then predicting the response by

$$\dot{\mathbf{u}}_{n+1} = \dot{\mathbf{u}}_n + \Delta t \ddot{\mathbf{u}}_n, \qquad \mathbf{u}_{n+1} = \mathbf{u}_n + \Delta t \dot{\mathbf{u}}_{n+1} \tag{12}$$

where $\mathbf{u}$ is the displacement. The solution procedure for the uncoupled thermo-mechanical problem is sketched in Table 2.

Table 1. Solution procedure for the thermo-mechanical problem (computations during each time step n)

1. Solve for the temperature $\boldsymbol{\theta}_{n+1}$ from equation (11)

2. By looping over all the elements, solve the model defined by equations (4)-(8) for displacement jump $\boldsymbol{\alpha}_d$ and the internal variables, calculate the new stress $\boldsymbol{\sigma}$ by equation (9), and assemble the internal force vector (3)

3. Solve for the acceleration $\ddot{\mathbf{u}}_n$ from equation (3)

4. Predict the mechanical response by equations (12)

6 Simulation results and discussion

Here we present some representative simulations of compressive tests performed on heat shocked numerical rock samples (Figure 1 a-b) generated with the method illustrated in Section 3. The boundary conditions for the thermal problem, i.e. the heat shock, are defined as a constant flux q at the left and right edges of the numerical sample. The initial temperature in the sample is $20°$ C. For the consequent uniaxial compression test, the mechanical boundary conditions characterize the sample as simply supported at the bottom, with a constant velocity of 0.1 m/s at the top edge (Figure 1 a-b). The material properties are given in Table 2.

Table 2. Material properties and model parameters used in simulations

	Parameter		Quartz	Feldspar	Biotite
	Percentage in the sample	[%]	33	50	17
ρ	(Density)	[kg/m^3]	2.65	2.62	3.05
E	(Elastic modulus)	[GPa]	80	60	20
ν	(Poisson's ratio)		0.17	0.29	0.20
σ_t	(Tensile strength)	[MPa]	10	8	7
σ_s	(Shear strength)	[MPa]	50	50	50
φ	(Internal friction angle)	[°]	50	50	50
G_{Ic}	(Mode I fracture energy)	[J/m^2]	40	40	28
α	(Thermal expansion coefficient)	[1/K]	1.60×10^{-5}	0.75×10^{-5}	1.21×10^{-5}
k	(Thermal conductivity)	[W/mK]	4.94	2.34	3.14
c	(Specific heat capacity)	[J/kgK]	731	730	770

The mineral properties are mainly from (Park et al., 2015). It should be noted that the properties do not necessarily represent any single real rock, but still are representative for granitic rocks. Moreover, the temperature dependance is neglected. Finally, the viscosity value is set to 0.005 MPa·s/m.
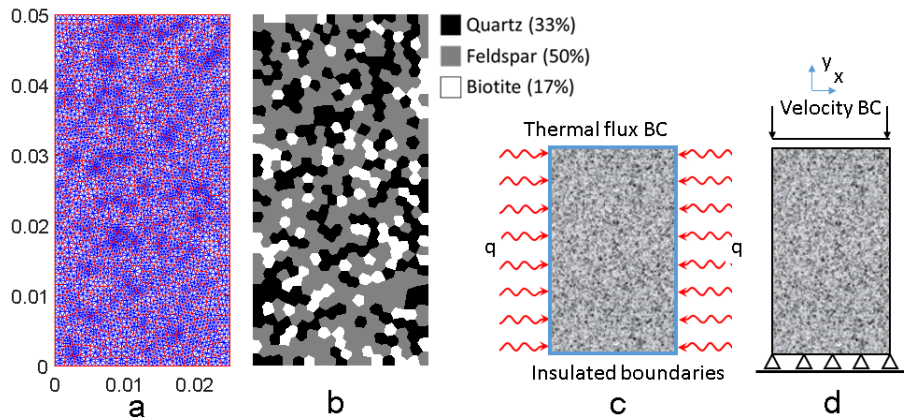
Figure 1. FE mesh and centroidal Voronoi tessellation for the numerical rock sample a-b), boundary conditions for the heat shock test c) and the compression test d).

In Figure 2 results for the heat-shock simulation are shown. While there is a substantial increase in temperature at the boundary nodes, most part of numerical sample remains at the reference temperature due to the very short duration of the heat shock. A significant amount of heat induced cracks can be observed at the boundaries of the specimen. However, the crack openings are quite small (Figure 2 b).
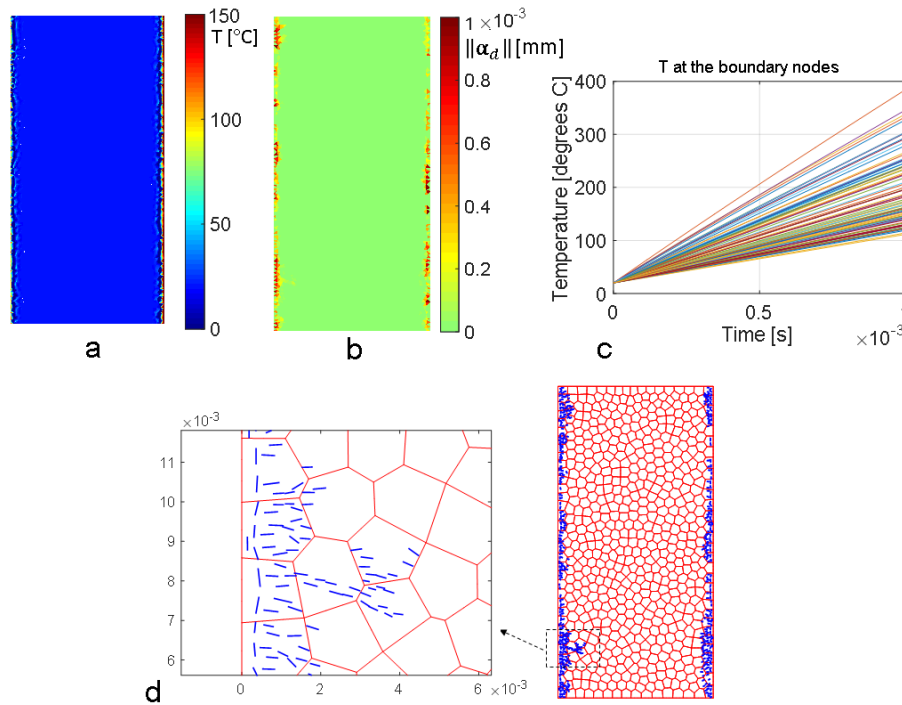
Figure 2. Simulation results for heat shock: temperature distribution a), displacement jump distribution b), temperatures at the boundary nodes c) and orientation of the thermal shock induced cracks in the sample d).

Figure 3 a-c) presents the failure modes in the uniaxial compression tests for three different cases: intact rock sample a); sample cooled down to room temperature b); sample mechanically loaded immediately after the heat shock c).

The failure modes in cases a) and b) are quite similar, but c) deviates substantially due to the highly disturbed initial stress state. Figure 3 d) shows the average stress-strain curves for the corresponding three cases. The resulting compressive strength for case b) and c) show a reduction in strenght of, respectively, 35% and 50%, compared to the strength of the intact rock ($\sim$ 180 MPa).
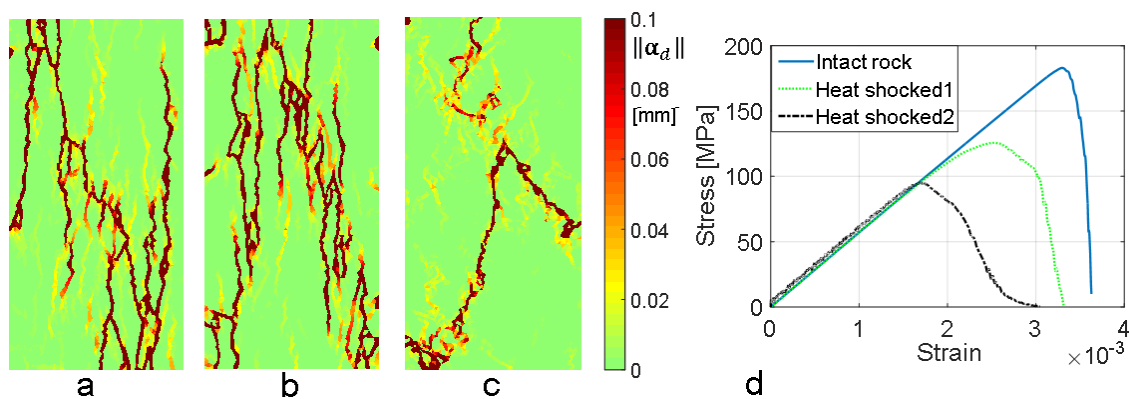
Figure 3. Simulation results for compression tests: final failures mode for intact rock a), heat shocked, cooled down case b), heat shocked and immediate compression c), average stress-strain curves for the three cases d).

7 Conclusions

A 2D numerical approach for modelling the heat shock-induced damage in the granitic rock was introduced in this paper. As the model is based on the embedded-discontinuity finite elements, it can account for the microcrack orientations induced by the heat shock modelled as a lateral heat flux applied at the vertical boundaries of the numerical specimen. Despite the fact that the cracks were limited in a very narrow zones close to the boundaries, significant reduction (35% to 50%) in the compressive strength of the intact rock was observed in the samples. Therefore, the short-duration high-intensity heat flux provides an efficient means to enhance mechanical breakage of rock. This method will be applied in numerical modelling of heat shock enhanced percussive drilling. Moreover, the effect of temperature dependance of the mechanical and thermal properties of the rock constituting minerals needs to be addressed in the future studies of the method.

Acknowledgments

References

Mardoukhi A., Saksala T., Hokka M. and Kuokkala V.- T., A numerical and experimental study in the tensile behavior of plasma shocked granite under dynamic loading. *Rakenteiden Mekaniikka (Journal of Structural Mechanics)*, vol. 50, pp. 41–62, 2017.

Park J.-W., Park C., Ryu D. and Park E.S., Numerical simulation of thermo-mechanical behavior of rock using a grain-based distinct element model. *In: Schubert & Kluckner (Ed.). Proceedings of EUROCK 2015 & 64th Geomechanics Colloquium.*, Salzburg, Austria, 2015.

Saksala T., Brancherie D., Harari I. and Ibrahimbegovic A., Combined continuum damage-embedded discontinuity model for explicit dynamic fracture analyses of quasi-brittle materials. *International Journal for Numerical Methods in Engineering*, vol. 101, pp. 230–250, 2015.

Talischi C., Paulino G. H. and Menezes I. F. M., PolyMesher: a general-purpose mesh generator for polygonal elements written in Matlab. *Structural and Multidisciplinary Optimization*, vol. 45, pp. 309–328, 2012.

Walsh S. D. C. and Lomov I. N., Micromechanical modeling of thermal spallation in granitic rock. *International Journal of Heat and Mass Transfer*, vol. 65, pp. 366–373, 2013.

Whittles D. N., Kingman S. W. and Reddish D. J., Application of numerical modelling for prediction of the influence of power density on microwave-assisted breakage. *International Journal of Mineral Processing*, vol. 68, pp. 71–91, 2003.